Post-Translational Tubulin Modifications in Differentiated Human Neural Stem Cells

V. Bleu Knight, Manasi P. Jogalekar, *Elba E. Serrano

Department of Biology, New Mexico State University, Las Cruces, NM, 88003 USA

Corresponding Author:

Elba E. Serrano

Department of Biology, New Mexico State University, Las Cruces, NM, 88003 USA

Email address: serrano@nmsu.edu

Keywords

tubulin; astrocyte; neuroglia; acetylation; glutamylation; astrocyte; immunocytochemistry; post-translational modifications; stem cell; tubulin code

Abbreviations

β – beta

BSA – bovine serum albumin

hESC- human embryonic stem cell

hNSC- human neural stem cell

IgG – immunoglobulin

MAP – microtubule associated protein

PBS – phosphate buffered saline

PBST – phosphate buffered saline with 0.1% TWEEN® 20

RRID – Research Resource Identifiers

PTM - Post-translational modifications

ABSTRACT

The tubulin protein fulfills a variety of cellular functions that range from chromosomal separation to locomotion. The functional diversity of tubulin is achieved through the expression of tubulin isotypes in different cell types or developmental time periods. Post-translational modifications (PTMs) of tubulin also are vital for specific intracellular tasks, such as binding and recruiting motor proteins. In neurons, the isotypic expression profile for tubulin is well characterized, and the importance of PTMs for proper neuronal function has gained recent attention due to their implication in neurodegenerative disorders. In contrast, the role of tubulin specializations in the determination of neural cell fate has received minimal attention and studies of tubulin PTMs and isotypes in neuroglia such as astrocytes are relatively few. To bridge this knowledge gap, we undertook an analysis of PTMs in neurons and astrocytes derived from the federally approved H9 hESC-derived human neural stem cell (hNSC) line. In hNSCs, basal cells can be directed to assume neural fate as neurons or astrocytes by specifying different media growth conditions. Immunocytochemical methods, fluorescent antibody probes, and confocal microscopy facilitated image acquisition of fluorescent signals from class III β- tubulin (βIII-tubulin), polyglutamylated tubulin, and acetylated tubulin. The EBImage package for the statistical programming language R was used to assess and compare fluorescent probe intensities using Student's t-tests. Qualitative analysis indicated that βIII-tubulin, polyglutamylated tubulin, and acetylated tubulin were expressed to some degree in basal hNSCs and their media-differentiated hNSC neuronal and astroglial progeny. In media-differentiated hNSC astrocyte progeny, quantification and statistical analysis of fluorescence probe intensities showed that acetylated tubulin/ βIII-tubulin ratios were greater than polyglutamylated tubulin/ βIII-tubulin ratios. These findings represent a snapshot of the dynamic and varied changes tubulin expression profile during the specification of neural cell identity. Results imply that investigations of tubulin PTMs have the potential to further understanding of the generation and regeneration of nervous tissue.

1. INTRODUCTION

The protein tubulin is abundant in most cells and fulfils specific functions within each cell. Tubulin specializations have been ascribed to isotypic expression profiles and modifications of tubulin that follow protein translation and that are described as the 'tubulin code' (Janke, 2014; Janke and Magiera, 2020; Roll-Mecak, 2020). The extensive variety of potential tubulin proteins that can be encoded give rise to the complexity of tubulin functions, which include chromosomal separation, intracellular transport, and cell structure, among others (Chakraborti et al., 2016; Li and Yang, 2015). PTMs of tubulin, such as acetylation, glutamylation, tyrosination, and glycylation occur enzymatically and serve to confer specific molecular functions (Pellegrini et al., 2017; Roll-Mecak, 2020; Song and Brady, 2015;). Moreover, the alpha and beta isotypic profiles vary according to cell and tissue type, as well as developmental age (Lee et al., 1990; Tischfield et al. 2011).

The significance of deciphering the tubulin code has been recognized, and many investigations have been undertaken to advance this effort (Audebert et al., 1993; Cambray-Deakin and Burgoyne, 1987; Janke and Kneussel, 2010; Lee et al., 1990; Romaniello et al., 2015; Saragoni et al., 2000; Zhang et al., 2015). Translation of the tubulin code is particularly important for central nervous system research because of the putative relationships between posttranslational tubulin modifications with CNS disorders, including Rett Syndrome, Epilepsy, Alzheimer's disease, and Parkinson's disease (Delépine et al., 2016; Saragoni et al, 2000; Zhang et al., 2015; Vu et al., 2017). In contrast with knowledge of PTMs in neural tissue, the isotypic expression profile of tubulin has been studied in greater detail.

Posttranslational tubulin modifications confer specific microtubule specializations in the nervous system. Acetylated neuronal tubulin has been implicated in protein-protein interactions and the trafficking and recruitment of motor proteins depends on the acetylation of microtubules (Pellegrini et al., 2017). Polyglutamylation also affects motor proteins through a demonstrated role in motor protein binding (Lessard et al. 2019). Modification of microtubule associated protein (MAP) is linked to polyglutamylation of tubulin in neurons, and acetylation has a putative role in neuronal plasticity (Moutin et al., 2021). Moreover, the asymmetrical functionalization of microtubules in soma, dendrites, axons, and growth cones through posttranslational glutamylation, acetylation, and tyrosination of microtubules helps establish the architectural polarity that is characteristic of neurons (Park and Roll-Mecak, 2018). Although investigations of posttranslational tubulin modifications in glia are limited, acetylation, and, to a lesser degree, polyglutamylation have been demonstrated in cultured human astrocytes (Knight and Serrano, 2017c). While acetylation and polyglutamylation both occur in cultured rat Schwann cells, polyglutamylation is more prevalent in these glial cells (Gadau, 2015). Astrocytic PTMs of tubulin play a putative role in regulation of the Na^+/ K^+ ATPase, neurodegeneration, and the inflammatory response (Casale et al., 2003; Yoshiyama et al., 2003; Youn et al., 2015). These studies show that distinct posttranslational modification profiles are necessary for tubulin function within the nervous system and highlight the need for a detailed characterization

of the tubulin code in neurons and neuroglia during normal development as well as in neural diseases and disorders (Roll-Mecak, 2020).

The Class III β-tubulin isotype (βIII-tubulin), which is synonymous with neuron specific β-tubulin, is commonly used as a biomarker to identify neuronal differentiation. However, the use of βIII-tubulin in this regard has been scrutinized because its expression is observed in other neural cell types. In particular, βIII-tubulin has been demonstrated in distinct populations of human astrocytes, including astrocytes of fetal origin, as well as mature astrocytes after injury or neoplastic transformation (Dráberová et al., 2008; Katsetos et al., 2001, 2002; Knight and Serrano, 2017a). In H9-derived human neural stem cells (hNSC), the expression of βIII-tubulin increases with the expansion of basal cells, and is observed in cultures grown in neuronal and astroglial differentiation conditions (Oikari et al., 2016). Thus, the isotypic expression pattern of βIII-tubulin appears to intersect the boundary between neurons and astrocytes. The promiscuous expression of βIII-tubulin and other differentiation markers among neural cell types has prompted the exploration of alternative molecules to describe cell fate determination (Oikari et al., 2016). PTMs of tubulin, specifically acetylation and polyglutamylation, are reportedly upregulated in neurons, and therefore offer the potential to enhance the use of βIII-tubulin as a neuronal marker.

While posttranslational tubulin modifications have been explored in the pre-implantation embryo and through the development of knockout mice, much less is known about the posttranslational modification profiles of tubulin in differentiating stem cells (Houliston and Maro, 1989; Zhang et al., 2008). The exploration of PTMs in differentiating stem cells may reveal specializations of tubulin that occur during the determination of cell fate. To fill this knowledge gap, we evaluated the occurrence of two tubulin PTMs, glutamylation and acetylation, in the H9-derived human neural stem cell line (hNSC) under three media growth conditions: basal, neuronal differentiation, and astroglial differentiation. To enhance reproducibility, we designed experiments that implemented immunocytochemical methods that relied on antibodies characterized in the Research Resource Identifiers (RRID) registry (Bandrowski et al., 2016). Our results offer insight into the posttranslational modification profile of tubulin during specification of neural cell fate in an *in vitro* system.

2. METHODS

2.1 Cell culture

Gibco® H9 hESC-Derived Human Neural Stem Cells (hNSC; ThermoFisher Scientific, N7800100; lot 1402001; RRID CVCL_IU37) were cultured according to the manufacturer's specifications for basal cell culture, as well as neuronal and astroglial differentiation. Complete hNSC serum free media for basal cell culture contained Knockout DMEM/F-12 (97%; Gibco®, 12660-012), GlutaMAX™ (1%; Gibco®, 35050-061), StemPro neural supplement (2%; Gibco®, A10508), bFGF (2 µg / 100 mL; Gibco®, PH60024), and EGF (2 µg / 100 mL; Gibco®, PHG0314). Prior to aliquoting, media were filtered through a 0.2 µm porous membrane.

The T-25 flasks used for basal expansion and the 24- or 96- well plates used for imaging basal cells and differentiated astrocytes were coated with Geltrex™ Reduced Growth Factor Basement Membrane Matrix (Gibco®, 12760; (1:200) for one hour at room temperature. Prior to the addition of cells, Geltrex™ -coated flasks and plates were rinsed with Dulbecco's modified PBS (DPBS) that included calcium and magnesium, as recommended by the manufacturer. The 24- or 96- well plates used for neuronal differentiation were coated with poly-L-ornithine (Sigma-Aldrich, P3655; 20 µg/mL) overnight at room temperature (~26°C), then rinsed twice in sterile water before coating with laminin (Gibco®, 23017-015; 10 µg/mL) for two hours at 37°C, 5% CO_2. Prior to the addition of cells, double ornithine/ laminin coated flasks and plates were rinsed with (DPBS) without added calcium or magnesium, as recommended by the manufacturer.

Ampules of frozen cells were thawed, transferred to sterile centrifuge tubes (15 ml) with media (8ml) and centrifuged at 210 G (3 min). Cryoprotectant was removed by withdrawing all but 1 mL of media and the cell pellet was resuspended in media, then plated into flasks coated with Geltrex™ (~8 x 10^4 cells/ cm^2; one T25 flask per ampule,). Flasks with hNSCs (passage 0) were maintained in an incubator at 37°C, 5% CO_2. Media were replenished in basal cultures every 48 hours. Cells were subcultured according to the manufacturer's specifications when cultures reached 80% confluence (day 2 for new vials). After removal of the media, cells were rinsed in DPBS with no magnesium or calcium, then 2 mL of pre-warmed StemPRO Accutase (Gibco®, A11105-01) was added to each flask. When cell detachment was confirmed under the microscope, cells were transferred to centrifuge tubes with 9 ml of media, then centrifuged at 210G (3 min). Media were removed until the cell pellet was covered by 1 mL of the supernatant. Cells were resuspended by titration after the addition of 2 ml of prewarmed media.

The first and second passages were used to initiate neuronal and astrocytic differentiation, and for imaging of basal cells. Passaged cells were plated in complete hNSC serum free media, and differentiation was initiated after attachment, between 24 and 48 hours after plating.

Neuronal differentiation was initiated by replacing media with neuronal differentiation media, prepared according to manufacturer's specifications with 97 mL of Neurobasal® Medium (Gibco®, 21103), 2 mL of B-27® Serum-Free Supplement (Gibco®, 17504), and 1 mL of GlutaMAX™. Media were filter

sterilized with a 0.2 µm porous membrane and stored in 20 ml aliquots. Half media changes replenished cultures every three to four days. If confluence exceeded 75%, differentiated neuronal cultures were passaged, and passage of differentiated neurons was not undertaken past day 7 as recommended by the manufacturer. Differentiated neurons were split 1:2 between 0 and 2 times. Neurons were harvested at day 7, day 10, and day 14. For cultures that proceeded past 7 days, Dibutyryl cAMP (Sigma-Aldrich, D0627) was added for a final concentration of 0.5 mM on days 7, 8, and 9.

Astrocyte differentiation was initiated by replacing media with astrocyte differentiation media, prepared according to manufacturer's specifications with 97 mL of Dulbecco's Modified Eagle Medium (ATCC, 30-2002), 1 mL of N-2 Supplement (Gibco®, 17502), 1 mL of fetal bovine serum (ATCC, 30-2020), and 1 mL of GlutaMAX™. Media were filter sterilized with a 0.2 µm porous membrane and stored in 20 ml aliquots. Half media changes replenished the cultures every three to four days. If confluence exceeded 75%, differentiated astrocyte cultures were passaged. Differentiated astrocytes were passaged and divided in a 1:3 ratio between 1 and 4 times during the 21-day course of astrocyte differentiation for all cultures, as recommended by the manufacturer.

2.2 Live cell imaging with phase contrast microscopy

Phase contrast images of live samples were captured prior to cell fixation with Metavue image software (Molecular Devices) in conjunction with a Coolsnap HQ CCD camera (Photometrics). A 20X objective with a correction collar was used to visualize cells with an inverted Nikon TE-2000 microscope.

2.3 Antibody selection

βIII-tubulin was used as the reference target for our comparison of polyglutamylation and acetylation in hNSCs because studies report the expression of βIII-tubulin in basal hNSCs, as well as differentiated neurons and astrocytes (Oikari et al., 2016). βIII-tubulin was detected with rabbit anti-βIII-tubulin antibody (Abcam; catalog # ab52623, RRID:AB_869991).

Detection of polyglutamylation and acetylation parallel previous studies (Knight and Serrano, 2017c). The anti-polyglutamylated antibody used in this study came from the same mouse hybridoma clone (B3),but it was purchased from a different vendor (Sigma-Aldrich) than the version used in our previous analysis (Abcam). PTMs were labeled with mouse anti-polyglutamylated tubulin (Sigma-Aldrich; catalog # T9822, RRID:AB_477598), which putatively detects polyglutamylation of α- and β- tubulin isoforms and mouse anti-acetylated tubulin (Sigma-Aldrich; catalog # T7451, RRID:AB_609894), which putatively detects acetylation of the α- isoform. Antibodies were validated with Western blot analysis using protein from Neuronal Human Astrocytes (Lonza, CC-2565) as previously reported in Knight and Serrano (2017c).

2.5 Immunocytochemistry

Tubulin in hNSC cultures was labelled with immunocytochemical methods as reported previously (Knight and Serrano, 2017c). Specifically, primary antibodies were diluted to the following final concentrations: 1:300, rabbit anti-class III β- tubulin antibody; 1:200, mouse anti-polyglutamylated tubulin; 1:200, mouse anti-acetylated tubulin in PBST containing 1% Bovine Serum Albumin. Simultaneous incubation with rabbit anti-βIII-tubulin and either mouse anti-acetylated tubulin or mouse anti-polyglutamylated tubulin was used to label proteins. Alexa Fluor® 488-conjugated goat anti-rabbit IgG (Abcam; catalog # ab150077, RRID: AB_2630356) and Alexa Fluor® 594-conjugated goat anti-mouse IgG (Abcam; catalog # ab150120, RRID: AB_2631447) were simultaneously diluted at 1:500 in PBS with 1% BSA for secondary antibody exposure. Hoechst 33342 (0.1 µg/ ml) counterstained cell nuclei prior to mounting slides.

Immunocytochemistry controls were incorporated into the protocol. The specificity of the βIII-tubulin antibody was validated by incubating 1µg/ ml of the βIII-tubulin synthetic immunizing peptide with the diluted rabbit anti-class III β- tubulin antibody for one hour at ambient temperature (~26◦C) prior to overnight incubation followed by exposing samples to Alexa Fluor® 488-conjugated goat anti-rabbit IgG (Abcam; catalog # ab150077, RRID: AB_2630356) secondary antibody. The cross-reactivity of Alexa Fluor® 594-conjugated goat anti-mouse IgG and Alexa Fluor® 488-conjugated goat anti-rabbit IgG were assessed by incubating samples with only rabbit anti-class III β- tubulin (1:300), mouse anti-acetylated tubulin (1:200), or mouse anti-polyglutamylated tubulin (1:200). For the secondary antibody incubation, Alexa Fluor® 594-conjugated goat anti-mouse IgG (1:500) was incubated with samples exposed to the rabbit anti-class III β-tubulin antibody, and Alexa Fluor® 488-conjugated goat anti-rabbit IgG (1:500) was incubated with samples exposed to mouse anti-polyglutamylated tubulin (1:200), or mouse anti-acetylated tubulin (1:200).

2.6 Confocal imaging

Confocal images were acquired during multiple sessions using one of two LSM 700 confocal microscopes housed within the UTEP Border Biomedical Research Center (BBRC), depending on availability. Image capture settings were optimized based on control samples for each cell type (basal hNSCs, 7-day differentiated neurons, 10-day differentiated neurons, differentiated astrocytes (21 days) at each session (Table 1). Therefore, a variety of image capture settings and objectives were used. However, images of cells stained with acetylated tubulin and polyglutamylated tubulin were always captured in parallel, with identical settings, to facilitate a comparison of the posttranslational tubulin modifications in the same samples.

Images were captured with an EC Plan-Neofluar 10X/0.3 or EC Plan-Neofluar 20X/0.5 objective mounted on one of two inverted LSM 700 microscopes (Zeiss). Hoechst 33342 was excited with laser λ = 405 emission, Alexa Fluor® 488 was excited with laser λ = 488 emission, and Alexa Fluor® 594 was excited with laser λ = 555 emission. The LSM's main beamsplitter was configured for 405/488/555/639 wavelengths, with

variable dichroic beamsplitters at 579 nm, 587 nm, and 585 nm for tracks 1, 2, and 3, respectively. The SP 555 filter was used to collect emission from the first track (Hoechst), the SP 640 filter was used to collect emission from the second track (Alexa 488), and no filter was used in the third track.

Table 1. Confocal Image Acquisition Settings. Image capture parameters are reported for each imaging session, along with the number of images and the cell type(s) that were imaged in each session. Settings are given for the respective channels (1, 2, 3) and were consistent for each session. The # of stack images is given for each cell type and separated by comma.

Session	1	2	3	4	5	6
Laser Power (%)	5,5,5	5,2.2,5	11,5,5	5,5,5	7, 5, 5	13, 7, 11
Master Gain	850, 427, 507	850, 529, 529	739, 700, 705	850, 610, 775	850, 610, 775	972, 847, 864
Objective	20x, 63x	20x, 63x	20x	10x	10x	10x
Digital Gain	1	1	1	1	1	1
Digital Offset	0	0	0	0	0	0
Pinhole	1 AU	1AU	1AU	1AU	1AU	1AU
Cell Type (days in differentiation media)	Basal, Neuron (7)	Neuron (14)	Astrocytes (21)	Neuron (10)	Astrocytes (21), Neuron (10)	Astrocytes, Neuron (10)
# of Images (acetylated)	2, 5	2	3	7	5, 5	3,2
# of Images (polyglutamylated)	2, 3	2	3	7	5, 5	3,2

2.7 Fluorescence intensity analysis

Fluorescence intensity values were estimated in accordance with previously described methods (Knight and Serrano, 2017c). Maximum intensity projections were exported with a .tif extension using the Zeiss 2009 ZenLightEdition software package. Raw image .tif files were imported and translated into a 2 dimensional array values representing pixel intensity using the image processing package 'EBImage' for the R statistical programming language (Pau et al., 2010). Values ranged from 0 (black) to 1 (white) with a 16-bit range (216 values total).

PTMs (acetylation or polyglutamylation) were estimated for each image using the following ratios: the sum of fluorescent signal from the acetylated tubulin protein/ the sum of fluorescent signal from βIII-tubulin; or the sum of fluorescent signal from the polyglutamylated tubulin protein/ the sum of fluorescent signal from βIII-tubulin. The ratios were calculated for modified tubulin/ βIII-tubulin for all maximum intensity projection images from sessions 4 and 5 because of the identical image capture settings for channels 2 and 3, which captured fluorescent intensity from βIII-tubulin and modified tubulin, respectively.

Student's t-tests with a significance threshold (α) of 0.01 were used to evaluate possible differences in mean values of fluorescence intensity ratios. Comparisons of the ratios of acetylated and polyglutamylated tubulin to βIII-tubulin were made with data acquired from the same cell type (neurons or astrocytes). Comparisons of tubulin acetylation between neurons and astrocytes were made using the ratios of acetylated tubulin to βIII-tubulin for both cell types. Comparisons of tubulin polyglutamylation between neurons and astrocytes were made using the ratios of polyglutamylated tubulin to βIII-tubulin for both cell types. Statistical power was calculated as the ability to reject the null hypothesis (1- β) using G*Power version 3.1.9.2 (Faul et al., 2009).

2.8 Figure preparation

The relative contributions of fluorescence signals from each channel were manipulated with the Zeiss 2009 ZenLightEdition software package so that all signals were visible in the merged confocal images. Confocal images were also exported as TIFF files using the Zeiss 2009 ZenLightEdition software package. The image adjustment settings were consistent for all images in each figure and did not affect the data that were used for quantification purposes. Adobe CS6 Photoshop was used to align, label, and assemble images.

2.9 Rigor and reproducibility practices

Rigor and reproducibility guidelines proposed by the NIH were used as a model for these experiments (Landis et al., 2012). The hNSC line is derived from the NIH-approved WA09 (H9) embryonic stem cell line (NIHhESC-10-0062). Information about WA09 (H9) can be found in the NIH registry for human embryonic stem cells. The federally approved parent H9 (WA09) embryonic stem cell line was de-identified by NIH and is exempted from review by the NMSU Institutional Review Board.

hNSC differentiation was initiated within 3 passages (10 population doublings) to guarantee lineage according to the vendor specifications. The human origin of the cell line was confirmed through the alignment of the hNSC transcriptome to the human genome in RNA-seq experiments described previously (Knight and Serrano, 2017b). βIII-tubulin was detected with rabbit anti-βIII-tubulin antibody (Abcam; catalog # ab52623, RRID:AB_869991) that was validated through western blot analysis and by blocking with the immunizing peptide, as described previously (Knight and Serrano, 2017c).

3. RESULTS

3.1 Basal stem cells and their media-differentiated neuronal and astroglial hNSC progeny are characterized by morphological differences

Phase contrast images of basal and differentiated hNSCs revealed differences in cell size and structure. The basal stem cells (Fig. 1 A-C) appeared smaller in size than the differentiated astrocytes (Fig 1 D-F). Astrocytes appeared to branch and spread out in comparison to hNSCs, which demonstrated a compact morphology. Astrocytes were maintained in lower density cultures due to the tendency for endogenous growth factors to impede differentiation, and the necessity for those same growth factors to maintain stem cell pluripotency and prevent differentiation. Images of hNSC cultures (Figs. 1 and 2) reflect the recommended seeding density of 50,000 cells/ cm^2 for basal stem cells, and 25,000 cells/ cm^2 for astroglial differentiation, as well as the passage of astrocytes throughout differentiation when 80% confluence was attained. Despite the high seeding density of 50,000 cells/ cm^2, differentiated neurons were sparse in comparison to the basal hNSC cultures.

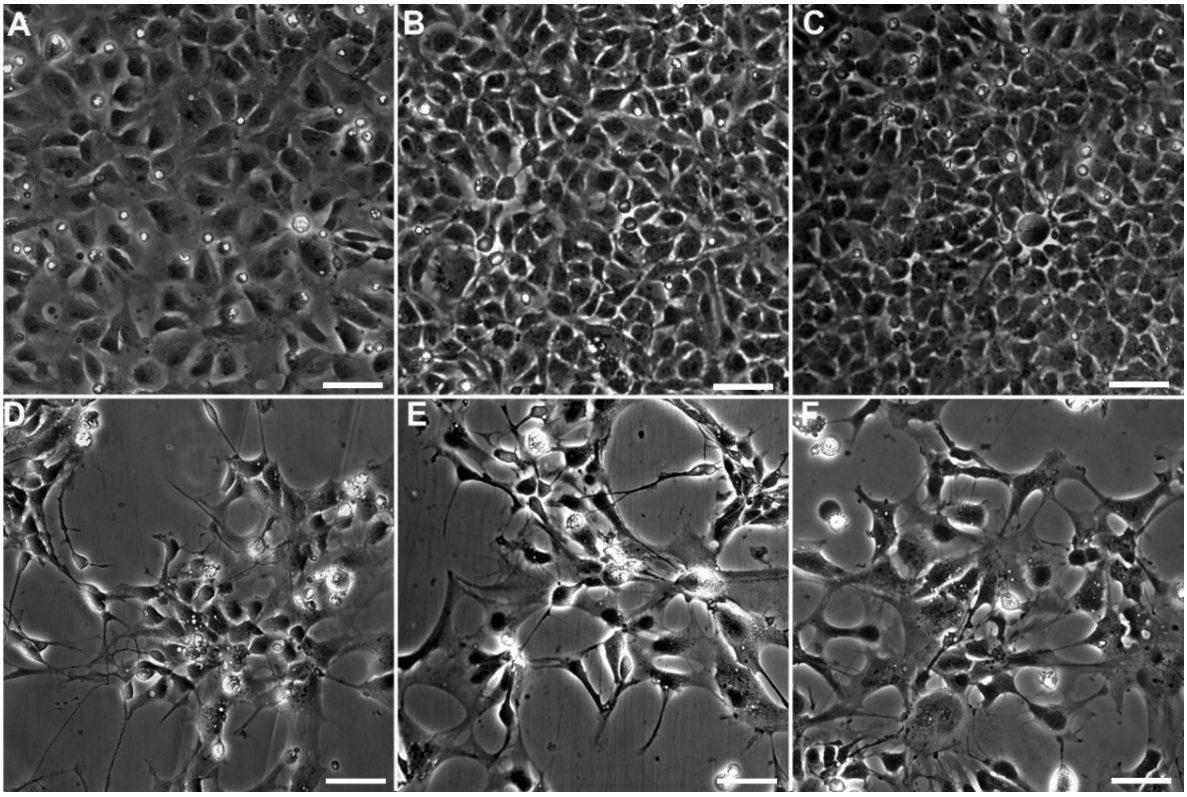

Figure 1. Basal hNSCs and Differentiated Astrocytes. Phase contrast images of live cells depict phenotypic differences between basal hNSCs 3 days after plating (A – C) and astrocytes exposed to differentiation conditions for 21 days (D – F). Scale bar = 50 µm.

Neuronal differentiation was assessed after 7 days, prior to the addition of cAMP (Fig. 2 A -C). The cultures were exposed to cAMP on days 7, 8, and 9, and assessment was undertaken on day 10 (Fig. 2 D-F), and day 14 (Fig. 2 G-I). The rounding up of hNSCs was seen after 7 days and became more prevalent as cultures progressed.

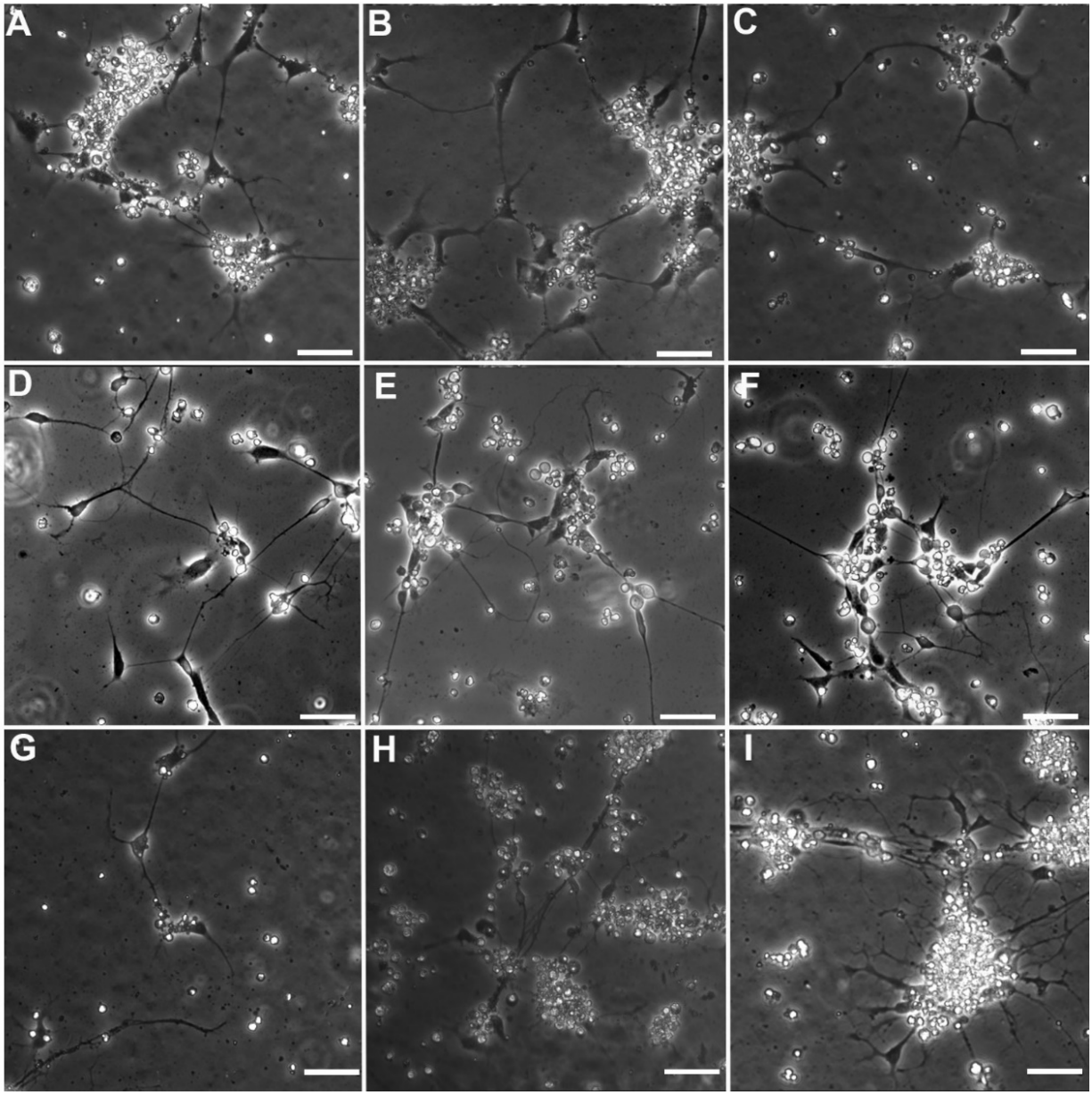

Figure 2 hNSCs in Neuronal Differentiation Conditions (1 – 4). Phase contrast images of live cells depict increased branching and polarization as neuronal differentiation progressed from day 7 (A -C) to day 10 (D-F) and day 14 (G-I). Phase bright cell bodies and polarization became apparent by day 10 (D-F). While polarization continued through 14 days of differentiation (G-I), phase bright cell bodies were less apparent in cultures after 14 days of differentiation conditions, and debris became prevalent. Scale bar = 50 µm.

Morphological assessments of basal and differentiated hNSCs were undertaken with phase contrast microscopy (Figs. 1 and 2). Basal hNSCs mandate a high seeding density and grow rapidly, thus they are densely packed and relatively small in comparison with differentiated astrocytes (Fig. 1).

After exposure to astrocyte differentiation media for 21 days, many cells become stellate, and some flatten out and spread to resemble the shape of fried eggs (Fig. 1). A qualitative assessment of neuronal differentiation does not show similar changes in the size of the cell body; however, long extensions protrude out of the cell body that become more extensive as differentiation proceeds (Fig. 2). After 7 days, the polarized phenotype that is typical of neurons was not always apparent in differentiated neurons (Fig. 2 A-C) In contrast, after 10 days, some cells appeared to adopt a polarized morphology, with a single dominant axon emerging from one side of the cell body (Fig. 2 D-F). After 14 days, debris became prevalent in the culture and phase-bright cell bodies were less apparent than in the cultures exposed to differentiation conditions for 10 days (Fig. 2 G-I). After 7 days, some cell bodies of differentiated neurons were phase bright, and while branching was evident, a qualitative assessment revealed that branching was not as extensive as compared to differentiated neurons after 10 and 14 days of exposure to neuronal differentiation conditions.

Our assessment of morphology at 7 days, 10 days, and 14 days after the initiation of neuronal differentiation led to a detailed, quantitative analysis of neuronal-differentiated cultures at day 10. We noted that although neurons and basal hNSCs are plated at the same initial seeding density, the cultures maintained in neuronal differentiation media begin to show signs of cell death and debris over time. Ten days following the initiation of neuronal differentiation, hNSC cultures assumed morphologies strongly resembling neurons, and retained the phase bright cell bodies that are indicative of healthy neuronal cultures.

3.2 Qualitative immunocytochemical characterization indicates expression of βIII-tubulin and tubulin PTM in basal stem cells and their media-differentiated neuronal and astroglial hNSC progeny

βIII-tubulin expression and the occurrence of post-translational acetylation and glutamylation in hNSC cultures were evaluated with immunocytochemical protocols. A βIII-tubulin positive label was observed in basal hNSCs and in cells cultured under all differentiation conditions (Fig. 3- 9). This result is consistent with prior reports of βIII-tubulin expression in hNSCs, human fetal astrocytes, and cultured neurons (Dráberová et al., 2008; Oikari et al., 2016; Knight and Serrano, 2017c). βIII-tubulin expression was consistently seen in hNSCs after 10 days of neuronal-differentiation as well as after astrocytic differentiation. A qualitative assessment of βIII-tubulin revealed an increase in expression as differentiation in basal hNSC cultures progressed to the astroglial or neuronal state.

In basal hNSC cultures, a qualitative assessment revealed that acetylation and polyglutamylation (Fig. 3) were both present, yet at low levels in comparison with differentiated cultures (Figs. 4- 9). Polyglutamylation appeared to be more prevalent than acetylation in basal hNSCs (Fig. 3). After seven days of neuronal differentiation, qualitative analysis indicated that acetylation (Fig. 4) was more prevalent than polyglutamylation (Fig. 5). In contrast, after 14 days of neuronal differentiation, polyglutamylation (Fig. 7) appeared more prevalent than acetylation (Fig. 6). After 21 days of astrocyte differentiation, acetylation (Fig. 8) appeared more prevalent than polyglutamylation (Fig. 9).

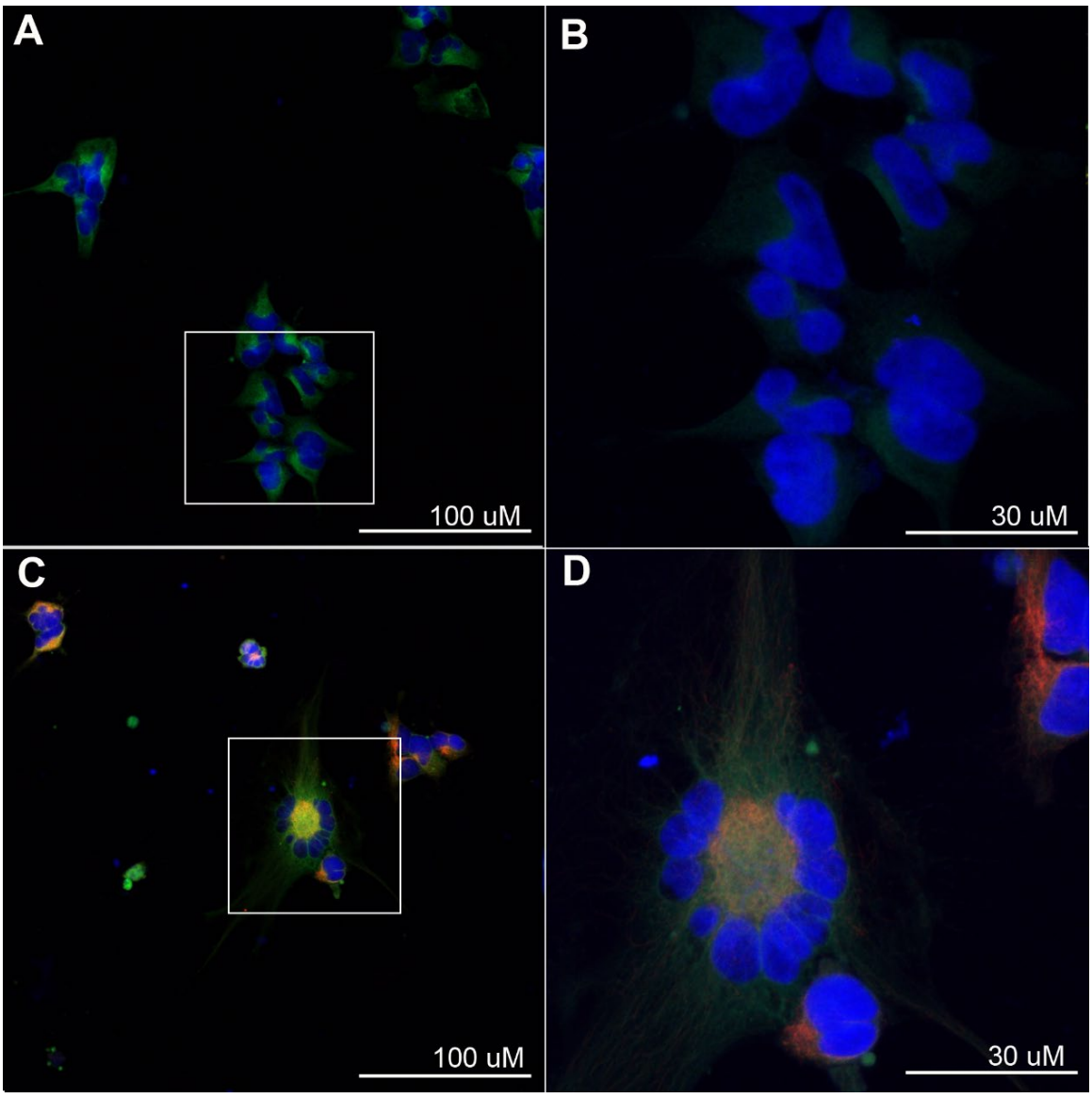

Figure 3. Acetylated, Polyglutamylated and βIII-tubulins in Basal hNSCs Fluorescent signals from nuclei (blue), βIII-tubulin (green), and acetylated (red, A, B) or polyglutamylated (red, C,D) tubulin were captured from basal (undifferentiated) hNSCs in single optical sections at 20x magnification (A, C) and z-series confocal stacks at 63x magnification (projections; B, D). Regions of image capture from higher magnification images are depicted in white boxes in A and C. Image contrast was enhanced to display fluorescent βIII-tubulin signal (85% contrast), polyglutamylated tubulin signal (A,B; 93% contrast), and acetylated tubulin signal (C,D; 93% contrast). Image capture settings and enhancements paralleled those for images of hNSCs after 7 days of neuronal differentiation (Figs. 4 and 5).

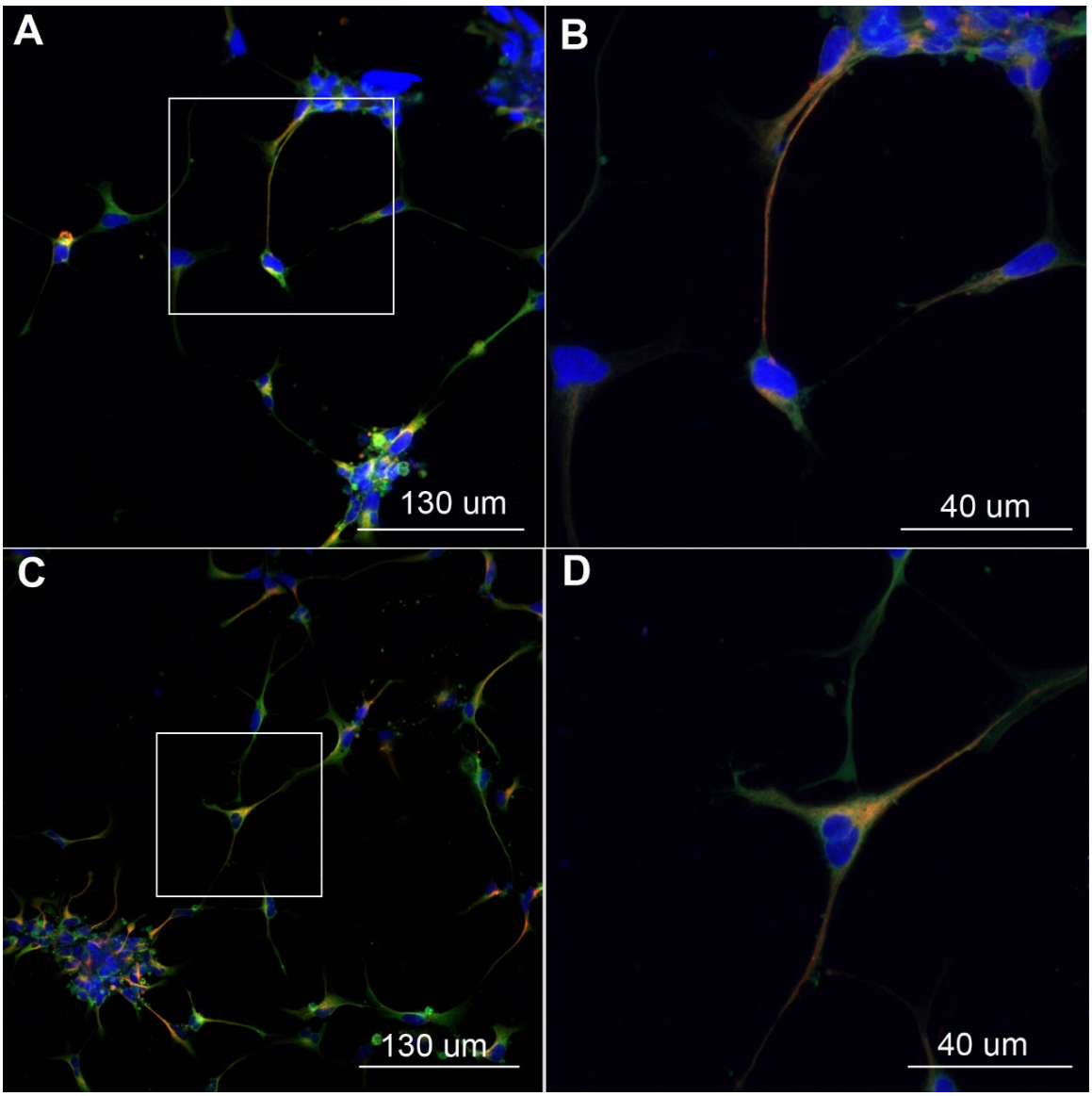

Figure 4. Acetylated Tubulin and βIII-tubulin in Differentiated Neurons (7 day) Fluorescent signals from nuclei (blue), βIII-tubulin (green), and acetylated (red, A, B) or polyglutamylated (red, C,D) tubulin were captured from hNSCs after 7 days of neuronal differentiation in single optical sections at 20x magnification (A, C) and z-series confocal stacks at 63x magnification (projections; B, D). Regions of image capture for higher magnification images are depicted in white boxes in A and C. Image contrast was enhanced to display fluorescent βIII-tubulin signal (75% contrast), and acetylated tubulin signal (93% contrast). Image capture settings and enhancements paralleled those for images of acetylated and polyglutamylated tubulin in basal hNSCs (Fig. 3), and after 7 days of neuronal differentiation (Fig. 5).

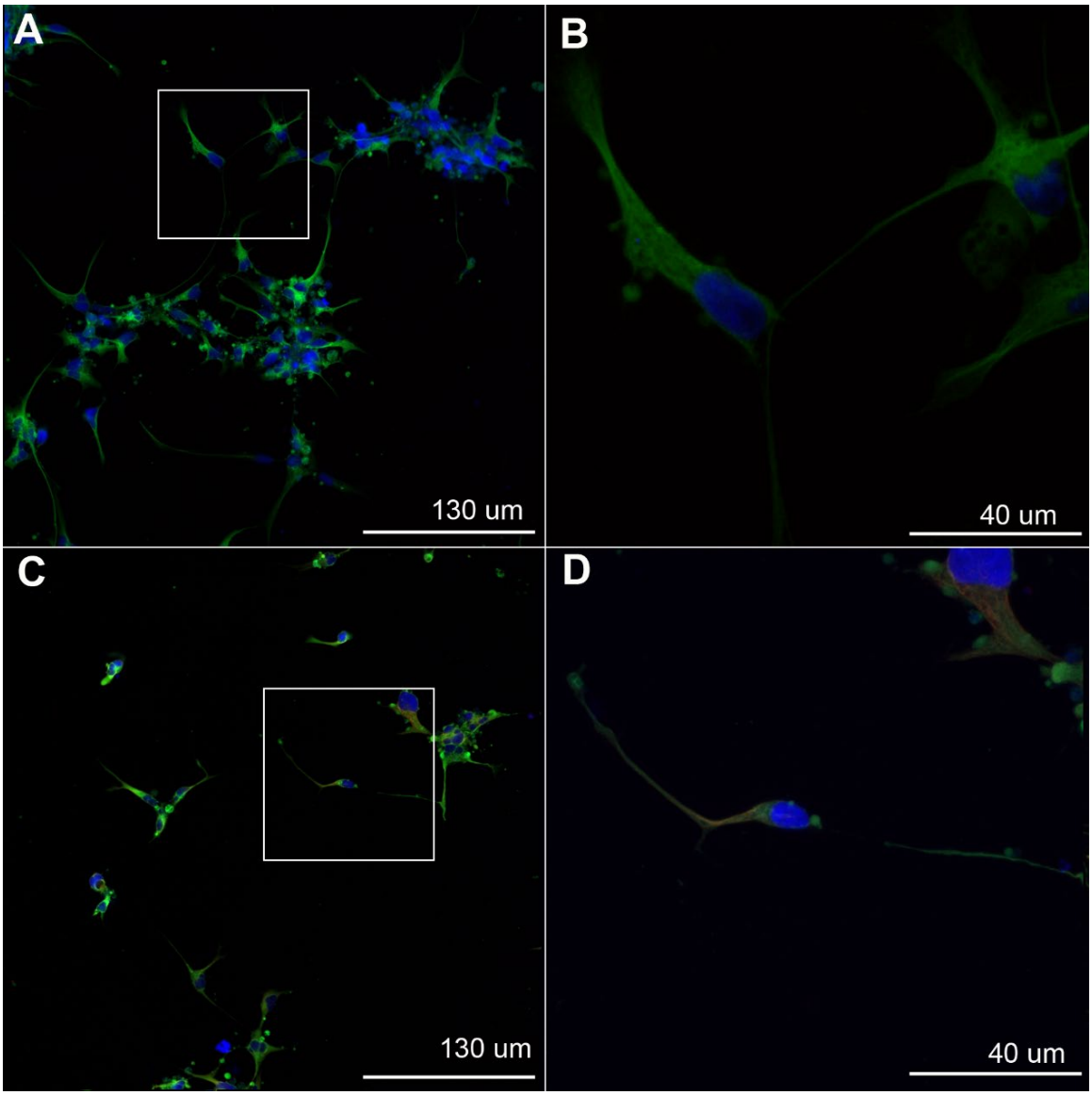

Figure 5. Polyglutamylated Tubulin and βIII-tubulin in Differentiated Neurons (7 day) Fluorescent signals from nuclei (blue), βIII-tubulin (green), and polyglutamylated (red, A, B) or polyglutamylated (red, C,D) tubulin were captured from hNSCs after 7 days of neuronal differentiation in single optical sections at 20x magnification (A, C) and z-series confocal stacks at 63x magnification (projections; B, D). Regions of image capture for higher magnification images are depicted in white boxes in A and C. Image contrast was enhanced to display fluorescent βIII-tubulin signal (75% contrast), and polyglutamylated tubulin signal (93% contrast). Image capture settings and enhancements paralleled those for images of polyglutamylated and acetylated tubulin in basal hNSCs (Fig. 3), and acetylated tubulin in hNSCs after 7 days of neuronal differentiation (Fig. 4).

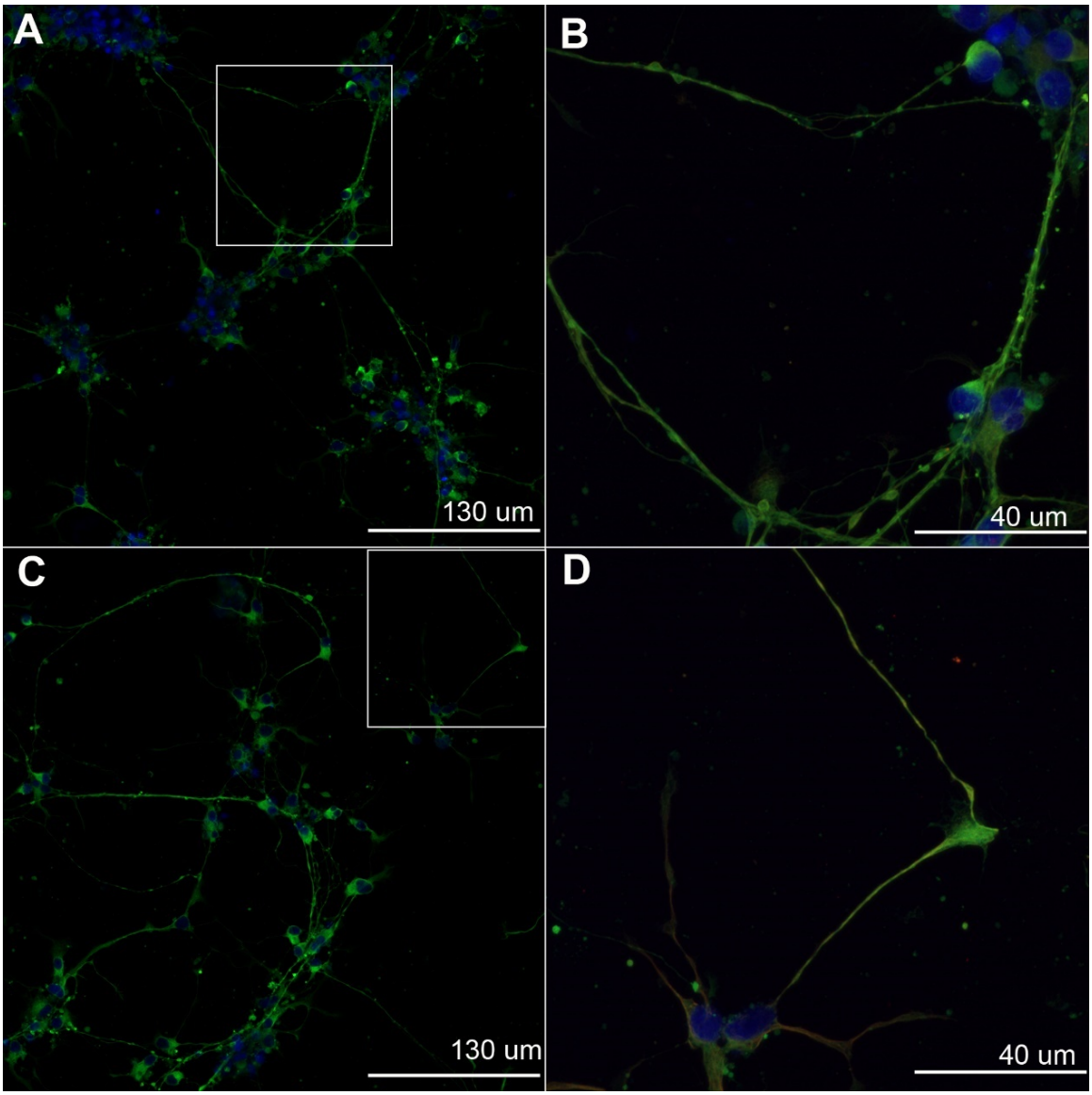

Figure 6. Acetylated Tubulin and βIII-tubulin in Differentiated Neurons (14 day) Fluorescent signals from nuclei (blue), βIII-tubulin (green), and acetylated tubulin (red) were captured from hNSCs after 14 days of neuronal differentiation in single optical sections at 20x magnification (A, C) and z-series confocal stacks at 63x magnification (projections; B, D). Regions of image capture for higher magnification images are depicted in white boxes in A and C. Image contrast was enhanced to display fluorescent βIII-tubulin signal (75% contrast), and acetylated tubulin signal (93% contrast). Image capture settings and enhancements paralleled those for images of polyglutamylated tubulin in hNSCs after 14 days of neuronal differentiation (Fig. 7).

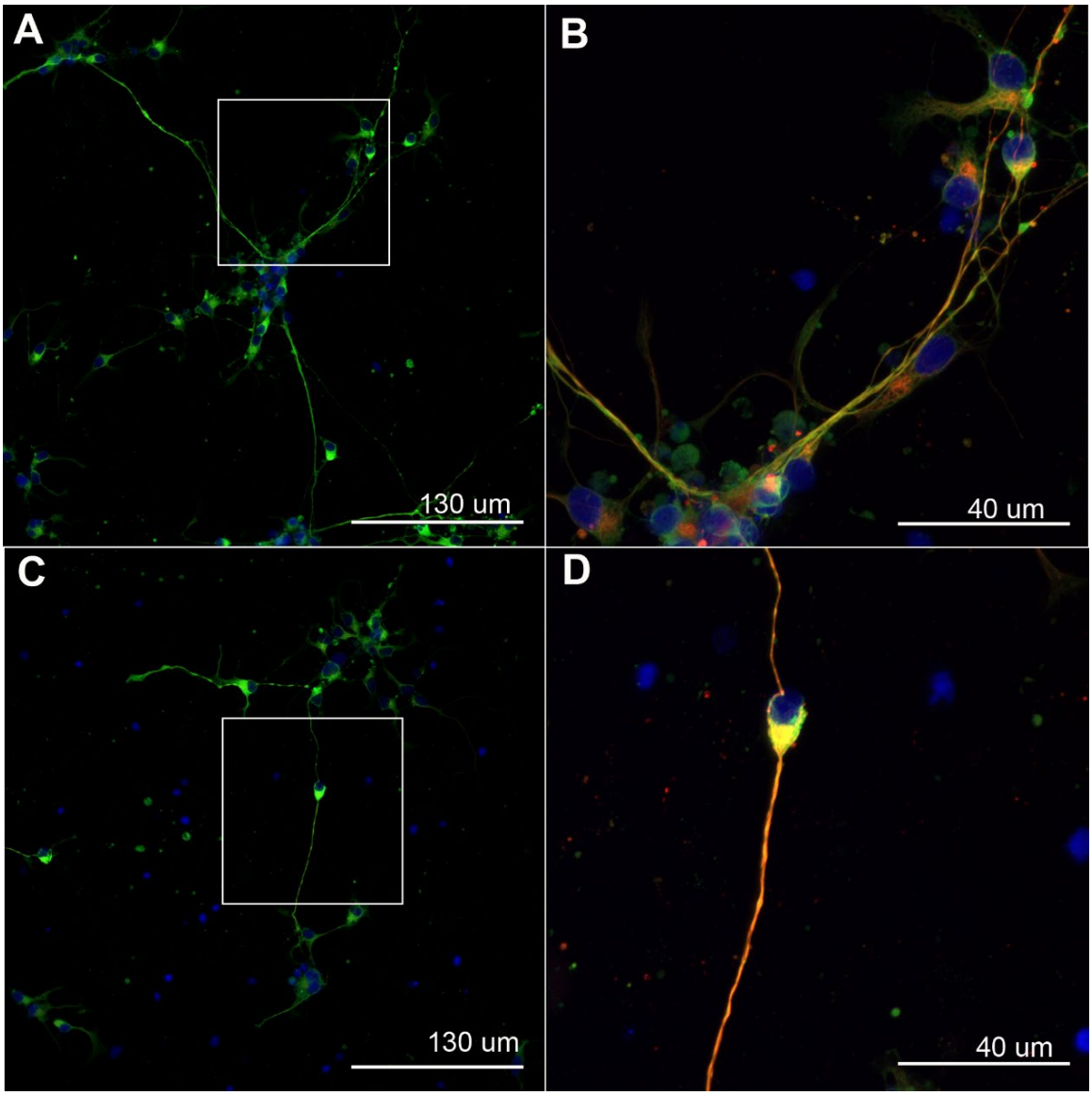

Figure 7. Polyglutamylated Tubulin and βIII-tubulin in Differentiated Neurons (14 day) Fluorescent signals from nuclei (blue), βIII-tubulin (green), and polyglutamylated tubulin (red) were captured from hNSCs after 14 days of neuronal differentiation in single optical sections at 20x magnification (A, C) and z-series confocal stacks at 63x magnification (projections; B, D). Regions of image capture from higher magnification images are depicted in white boxes in A and C. Image contrast was enhanced to display fluorescent βIII-tubulin signal (75% contrast), and polyglutamylated tubulin signal (93% contrast). Image capture settings and enhancements paralleled those for images of acetylated tubulin in hNSCs after 14 days of neuronal differentiation (Fig. 6).

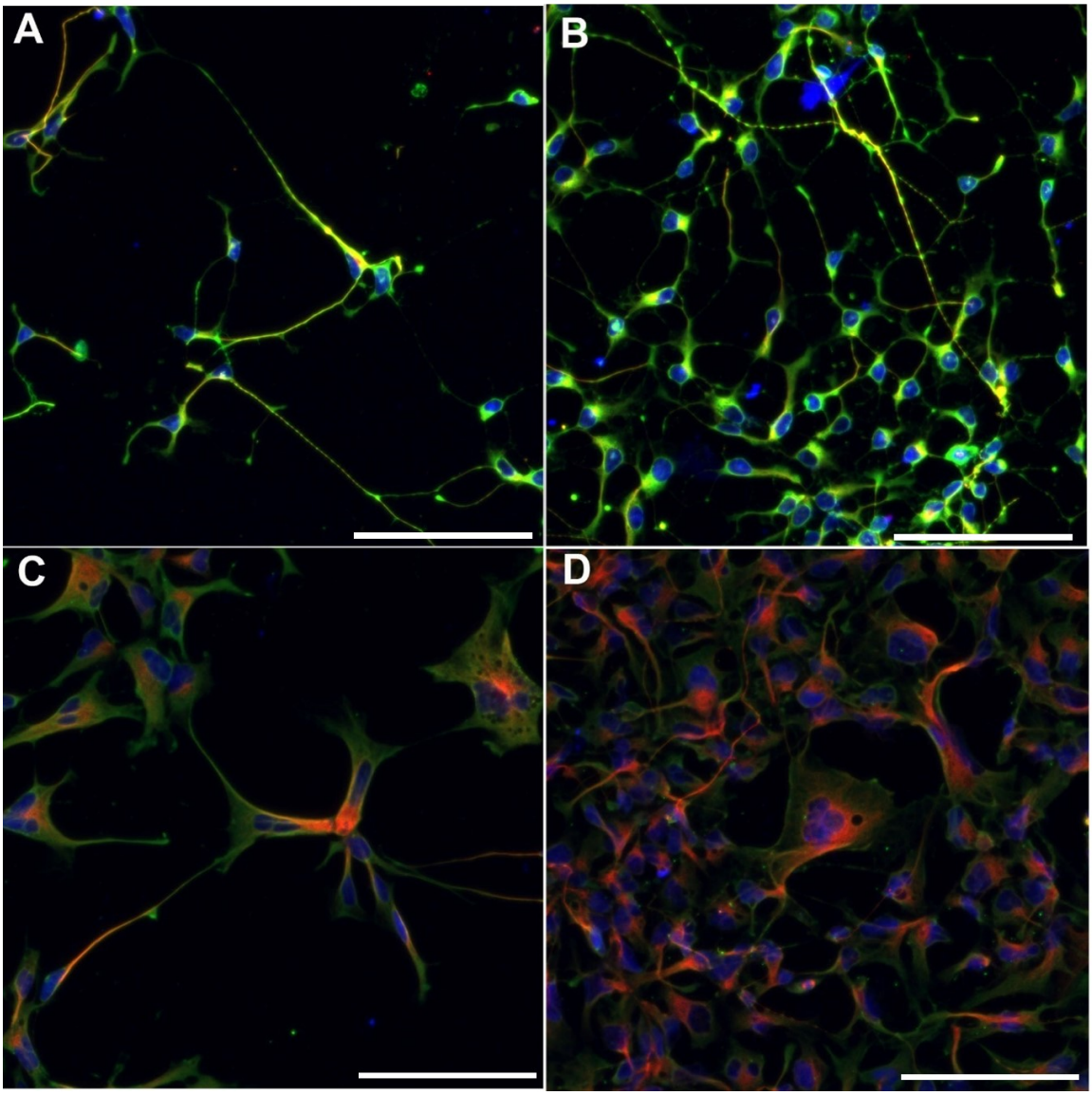

Figure 8 Acetylated Tubulin and βIII-tubulin in Differentiated Neurons (10 day) and Astrocytes Fluorescent signals from nuclei (blue), acetylated tubulin (red), and βIII-tubulin (green), were captured in z-series confocal stacks (maximum intensity projections displayed) from hNSCs after 10 days of neuronal differentiation (A, B) or 21 days of astroglial differentiation (C,D). Image contrast was not enhanced in the images. Image capture settings paralleled those for images of polyglutamylated tubulin in hNSCs after 10 days of neuronal and 21 days of astroglial differentiation (Fig. 9). Scale bar = 100 μm.

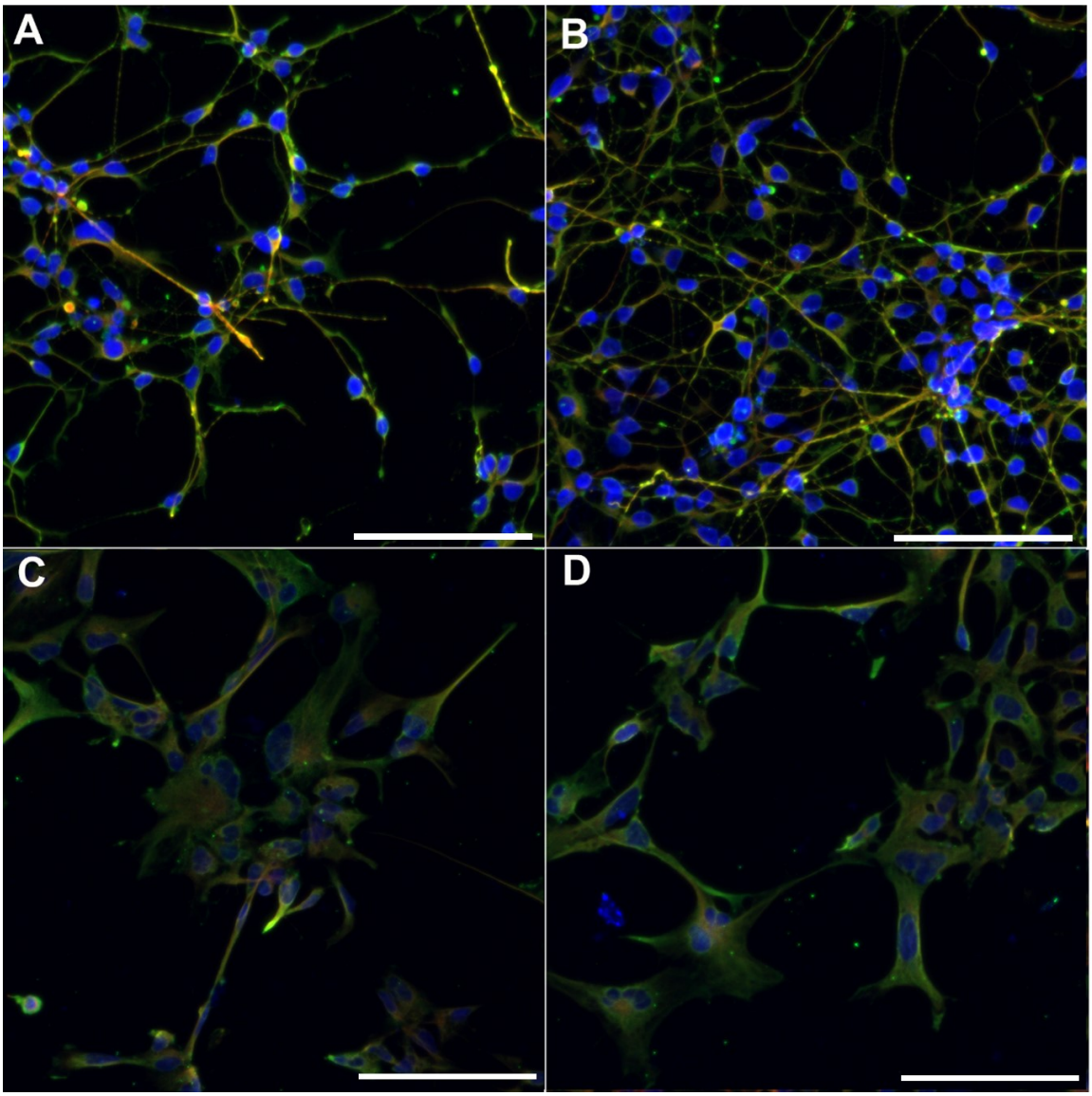

Figure 9 Polyglutamylated Tubulin and βIII-tubulin in Differentiated Neurons (10 day) and Astrocytes Fluorescent signals from nuclei (blue), polyglutamylated tubulin (red), and βIII-tubulin (green), were captured in z-series confocal stacks (maximum intensity projections displayed) from hNSCs after 10 days of neuronal differentiation (A, B) or 21 days of astroglial differentiation (C,D). Image brightness and contrast were not adjusted. Image capture settings paralleled those for images of acetylated tubulin in hNSCs after 10 days of neuronal and 21 days of astroglial differentiation (Fig. 8). Scale bar = 100 µm.

3.3 Quantitation of fluorescence intensity suggests differences in tubulin PTM between media-differentiated neuronal and astroglial hNSC progeny

Mean values for the ratios of PTM to βIII-tubulin were calculated for hNSC progeny after 10 days of neuronal differentiation and 21 days of astroglial differentiation. Acetylation and polyglutamylation were compared within each cell type (neurons, astrocytes). Potential differences in the level of each PTM (acetylation, polyglutamylation) between neurons and astrocytes were also evaluated.

The degree of tubulin post-translational modification (polyglutamylation or acetylation) was estimated using the ratio of the sum of fluorescent signal from polyglutamylated or acetylated tubulin to the sum of the βIII-tubulin fluorescent signal in each image.

Table 2. Statistical comparison of pixel intensity ratios for acetylated tubulin/ βIII-tubulin and polyglutamylated tubulin/ βIII-tubulin in hNSCs after 10 days of neuronal differentiation and 21 days of astrocytic differentiation. Images of neuronal (n=12) and astroglial (n = 5) progeny from sessions 4 and 5 (Table 1), where the magnification and master gain were identical (Table 2), were combined and evaluated for potential differences in posttranslational modifications. Students t-test unovered differences between the posttranslational tubulin modifications in astrocytes for polyglutamylation and acetylation with $p < 0.01$, denoted with *.

Test 1	**Cell Type**	**Mean**	**σ**	**T-value**	**DF**	**p Value**	**Power (1 – β)**
Acetylated Tubulin/ βIII-tubulin	Neurons	0.73	0.25	0.11	22	0.91	0.01
Polyglutamylated Tubulin/ βIII-tubulin	Neurons	0.72	0.12				
Test 2	**Cell Type**	**Mean**	**σ**	**T-value**	**D.F.**	**p Value**	**Power (1 – β)**
Acetylated Tubulin/ βIII-tubulin	Astrocytes	0.97	0.19	3.71	8	0.006*	1.00
Polyglutamylated Tubulin/ βIII-tubulin	Astrocytes	0.63	0.09				
Test 3	**Cell Type**	**Mean**	**σ**	**T-value**	**D.F.**	**p Value**	**Power (1 – β)**
Acetylated Tubulin/ βIII-tubulin	Neurons	0.73	0.25	1.95	16	0.07	0.37
Acetylated Tubulin/ βIII-tubulin	Astrocytes	0.97	0.19				
Test 4	**Cell Type**	**Mean**	**σ**	**T-value**	**D.F.**	**p Value**	**Power (1 – β)**
Polyglutamylated Tubulin/ βIII-tubulin	Neurons	0.72	0.12	1.50	16	0.15	0.21
Polyglutamylated Tubulin/ βIII-tubulin	Astrocytes	0.63	0.09				

The mean ratios for polyglutamylated tubulin/ βIII-tubulin acetylated and tubulin / βIII-tubulin were comparable in neurons (~0.7; Table 2). In astrocytes, a greater divergence was found between the mean ratios of acetylated tubulin/ βIII-tubulin (0.97) and polyglutamylated tubulin/ βIII-tubulin (0.63; $p < \alpha = 0.01$; Table 2). The mean ratio of polyglutamylated tubulin/ βIII-tubulin was 0.72 in neurons and 0.63 in astrocytes (Table 2). While the mean ratios of acetylated tubulin / βIII-tubulin in neurons (0.73) and astrocytes (0.97) were more divergent ($p > \alpha = 0.01$; Table 2).

4. DISCUSSION

Despite the current emphasis on the significance of posttranslational tubulin modifications in the central nervous system, tubulin acetylation and polyglutamylation patterns during the differentiation of neural stem cells have not been thoroughly explored (Cao et al., 2017; Sheikh et al. 2021). The expression of βIII-tubulin in neurons is well documented (Kapitein and Hoogenraad, 2015; Moody et al., 1989; Lee et al., 1990). There are relatively fewer demonstrations of βIII-tubulin expression in astrocytes and neural stem cells. However, the presence of βIII-tubulin is becoming established in human neural stem cells as well as plastic cell types and human fetal astrocytes (Dráberová et al., 2008; Katsetos et al., 2001, 2002, 2015; Knight and Serrano, 2017c; Oikari et al., 2016). Astrocytes are diverse and abundant in the CNS (Matias et al, 2019; Matyash and Kettenmann, 2010; Nedergaard et al, 2003; Oberheim et al., 2009; Stipursky et al., 2012). While the tubulin code has been credited with conferring the diverse array of functional specifications of tubulin, the exploration of potential connections between the tubulin code and astrocyte specialization is in its infancy. This research was an attempt to gain insight into tubulin specifications in human neural stem cells cultured in basal conditions and following differentiation into neurons and astrocytes. Immunocytochemical techniques were used to detect polyglutamylated tubulin, acetylated tubulin, and βIII-tubulin, in hNSCs.

We observed βIII-tubulin expression in hNSCs in all the culture conditions that were used in this study, a finding that is in accord with previous reports (Oikari et al., 2016). Quantification and statistical analysis of fluorescence intensity showed that probe intensity ratios for acetylated tubulin / βIII-tubulin and polyglutamylated tubulin/ βIII-tubulin were similar after 10 days of neuronal differentiation. In contrast, after astrocytic differentiation, the ratio of acetylated tubulin/ βIII-tubulin was greater than the ratio of polyglutamylated tubulin/ βIII-tubulin ($p < \alpha = 0.01$; Table 2). This finding is concordant with previous reports of more acetylation than polyglutamylation in human astrocytes (Knight and Serrano, 2017c).

Given that neurons and basal hNSCs are plated at the same initial seeding density, the neuronal differentiation conditions seem to impact the density of observed cells as seen in phase contrast images of basal hNSCs and neuronal progeny (Figs. 1 & 2). This could be attributed to the lack of division that characterizes cells that have committed to a neuronal lineage and are in a post-mitotic state (Deneris and Hobert, 2014; Herrup et al., 2004). Qualitative analysis indicated that acetylated tubulin and polyglutamylated

tubulin were also expressed in varying degrees throughout the course of neuronal differentiation. After seven days of differentiation, acetylation appeared more dominant than polyglutamylation in neuronal progeny (Figs. 4 & 5). After 10 days of differentiation, there is no distinct difference between the degrees of acetylation and polyglutamylation in neuronal progeny (Figs. 8 & 9). Finally, after 14 days of neuronal differentiation, polyglutamylation is more prevalent than acetylation in hNSC-derived neurons. This finding is contextualized by the increased levels of tubulin polyglutamylation that are seen in neurodegeneration, which increases in prevalence in proportion to age (Zempel et al., 2013; Vu et al., 2017; Santiago-Mujika et al., 2021; Bodakuntla et al., 2021). A putative role for polyglutamylated tubulin in neurodegenerative disorders is through the regulation of endoplasmic reticulum morphology (Zheng et al., 2021).

Whereas the link between polyglutamylation and neurodegeneration is being established, there is still relatively little information about the function of tubulin acetylation and polyglutamylation in the specification of neural cell fate (Moutin et al., 2021). The changing profile of tubulin modifications during neuronal development have been established in mouse neurons (Przyborski and Cambray-Deakin, Audebert et al., 1994). However, we have yet to understand the precise role of PTMs in the process of differentiation, particularly of human neural cell types. Acetylation and polyglutamylation have a demonstrated role in cell fate specification overall, as seen in the pre-implantation embryo and during mouse development (Houliston and Maro, 1989; Zhang et al., 2008). Recent studies have also established the role of acetylation in neuron development and morphogenesis, particularly with respect to axon overbranching (Wei et al., 2017). Our outcomes add to this accumulating evidence and advance the understanding of tubulin PTMs in human neurons and astrocytes during development.

In summary, these results are a preview of the tubulin modification patterns that facilitate the specification of distinct identities among neural cell types. Our findings offer insight into the complex specialization patterns conferred by tubulin PTMs in the specification of neural cell fate and the overarching process of morphogenesis. Outcomes from this study emphasize the need to explore how tubulin specifications contribute to neural cell identity during stem cell differentiation as well as the role of PMTs in glial functional diversity (Schiweck et al. 2018). Moreover, these findings present hNSCs and their progeny as a potential model for unraveling the complex processes of morphogenesis and neurodegeneration.

Author Contributions

V.B.K. conceived and designed the experiments, performed the experiments, analyzed the data, interpreted results, prepared the first draft of the manuscript, prepared all figures and/or tables, reviewed drafts of the paper. **M.P.J.** performed experiments and reviewed drafts of the paper. **E.E.S.** conceived and designed experiments, analyzed the data, interpreted results, contributed reagents/materials/analysis tools, co-wrote the paper, reviewed drafts of the paper, supervised project, provided oversight for compliance with institutional agency procedures for research integrity.

Funding.

This research received support from the New Mexico State University Endowment. Experiments used instruments and software at the University of Texas El Paso Border Biomedical Research Center is funded by the National Institute of Minority Health and Health Disparities of the National Institutes of Health (G12MD007592; MD007592).

Conflict of Interest.

The authors declare that they have no conflict of interest. The responsibility for the manuscript lies with the authors and content does not necessarily represent the official views of the National Institutes of Health or New Mexico State University.

Acknowledgement

We are grateful to Dr. Armando Varela-Ramirez for assistance with imaging experiments at the UTEP BBRC-CSIC Facility

5. REFERENCES

Audebert S., Koulakoff a., Berwald-Netter Y., Gros F., Denoulet P., & Eddé B. (1994). Developmental regulation of polyglutamylated alpha- and beta-tubulin in mouse brain neurons. *Journal of cell science* 107 (Pt 8:2313–22. DOI: 10.1016/j.ctrv.2012.07.005.

Bandrowski, A., Brush, M., Grethe, J. S., Haendel, M. A., Kennedy, D. N., Hill, S., Hof, P. R., Martone, M. E., Pols, M., Tan, S. C., Washington, N., Zudilova-Seinstra, E., & Vasilevsky, N. (2016). The Resource Identification Initiative: A Cultural Shift in Publishing. *The Journal of comparative neurology*, 524(1), 8–22. https://doi.org/10.1002/cne.23913

Bodakuntla, S., Yuan, X., Genova, M., Gadadhar, S., Leboucher, S., Birling, M. C., Klein, D., Martini, R., Janke, C., & Magiera, M. M. (2021). Distinct roles of α- and β-tubulin polyglutamylation in controlling axonal transport and in neurodegeneration. *The EMBO journal*, 40(17), e108498. https://doi.org/10.15252/embj.2021108498

Cambray-Deakin MA. & Burgoyne RD. (1987). Posttranslational modifications of α-tubulin: Acetylated and detyrosinated forms in axons of rat cerebellum. *Journal of Cell Biology* 104:1569–1574. DOI: 10.1083/jcb.104.6.1569.

Cao S, Du J, Lv Y, Lin H, Mao Z, Xu M, Liu M & Liu Y. PAX3 inhibits β-Tubulin-III expression and neuronal differentiation of neural stem cell. (2017). Biochem Biophys Res Commun. Apr 1;485(2):307-311. doi: 10.1016/j.bbrc.2017.02.086. Epub 2017 Feb 20. PMID: 28223217.

Casale CH., Previtali G. & Barra HS. (2003). Involvement of acetylated tubulin in the regulation of Na+,K+-ATPase activity in cultured astrocytes. *FEBS Letters* 534:115–118. DOI: 10.1016/S0014-5793(02)03802-4.

Chakraborti S., Natarajan K., Curiel J., Janke C. & Liu J. (2016). The emerging role of the tubulin code: from the tubulin molecule to neuronal function and disease. *Cytoskeleton (Hoboken, N.J.)*. DOI: 10.1002/cm.21290.

Delépine C., Meziane H., Nectoux J., Opitz M., Smith AB., Ballatore C., Saillour Y., Bennaceur-Griscelli A., Chang Q., Williams EC., Dahan M., Duboin A., Billuart P., Herault Y. & Bienvenu T. (2016). Altered microtubule dynamics and vesicular transport in mouse and human MeCP2-deficient astrocytes. *Human Molecular Genetics* 25:146–157. DOI: 10.1093/hmg/ddv464.

Deneris, E. S., & Hobert, O. (2014). Maintenance of postmitotic neuronal cell identity. Nature neuroscience, 17(7), 899–907. https://doi.org/10.1038/nn.3731

Dráberová E., Del Valle L., Gordon J., Marková V., Smejkalová B., Bertrand L., de Chadarévian J-P., Agamanolis DP., Legido A., Khalili K., Dráber P. & Katsetos CD. (2008). Class III beta-tubulin is constitutively coexpressed with glial fibrillary acidic protein and nestin in midgestational human fetal astrocytes: implications for phenotypic identity. *Journal of neuropathology and experimental neurology* 67:341–54. DOI: 10.1097/NEN.0b013e31816a686d.

Gadau SD. (2015). Detection, Distribution and Amount of Posttranslational α -Tubulin Modifications in Immortalized Rat Schwann Cells. *Archives italiennes de biologie*, *153*(4), 255–265. https://doi.org/10.12871/00039829201542.

Herrup, K., Neve, R., Ackerman, S. L., & Copani, A. (2004). Divide and die: cell cycle events as triggers of nerve cell death. *Journal of Neuroscience*, 24(42), 9232–9239. https://doi.org/10.1523/JNEUROSCI.3347-04.2004.

Houliston E. & Maro B. (1989). Posttranslational modification of distinct microtubule subpopulations during cell polarization and differentiation in the mouse preimplantation embryo. *Journal of Cell Biology* 108:543–551. DOI: 10.1083/jcb.108.2.543.

Janke C. (2014). The tubulin code: Molecular components, readout mechanisms, functions. *Journal of Cell Biology* 206:461–472. DOI: 10.1083/jcb.201406055.

Janke C. & Kneussel M.(2010). Tubulin post-translational modifications: Encoding functions on the neuronal microtubule cytoskeleton. *Trends in Neurosciences* 33:362–372. DOI: 10.1016/j.tins.2010.05.001.

Janke, C., & Magiera, M. M. (2020). The tubulin code and its role in controlling microtubule properties and functions. *Nature reviews. Molecular cell biology*, *21*(6), 307–326. https://doi.org/10.1038/s41580-020-0214-3

Kapitein, L. C. & Hoogenraad, C. C. (2015). Building the Neuronal Microtubule Cytoskeleton. *Neuron*, 87(3), 492–506. https://doi.org/10.1016/j.neuron.2015.05.046

Katsetos, C. D., Del Valle, L., Geddes, J. F., Aldape, K., Boyd, J. C., Legido, A., Khalili, K., Perentes, E., & Mörk, S. J. (2002). Localization of the neuronal class III beta-tubulin in oligodendrogliomas: comparison with Ki-67 proliferative index and 1p/19q status. *Journal of neuropathology and experimental neurology*, *61*(4), 307–320. https://doi.org/10.1093/jnen/61.4.307

Katsetos, C. D., Del Valle, L., Geddes, J. F., Assimakopoulou, M., Legido, A., Boyd, J. C., Balin, B., Parikh, N. A., Maraziotis, T., de Chadarevian, J. P., Varakis, J. N., Matsas, R., Spano, A., Frankfurter, A., Herman, M. M., & Khalili, K. (2001). Aberrant localization of the neuronal class III beta-tubulin in astrocytomas. *Archives of pathology & laboratory medicine*, 125(5), 613–624. https://doi.org/10.5858/2001-125-0613-ALOTNC

Katsetos C.D., Reginato MJ., Baas PW., D'Agostino L., Legido A., Tuszyn Ski JA., Dráberová E. & Dráber P. (2015). Emerging microtubule targets in glioma therapy. *Seminars in Pediatric Neurology* 22:49–72. DOI: 10.1016/j.spen.2015.03.009.

Knight VB., Serrano EE. (2017a). Hydrogel scaffolds promote neural gene expression and structural reorganization in human astrocyte cultures. *PeerJ*. DOI: 10.7717/peerj.2829.

Knight VB., Serrano EE. (2017b). RNA sequencing analysis of neural cell lines: impact of normalization and technical replication. In: Rojas I, Ortuño F eds. *Bioinformatics and Biomedical Engineering*. Granada: Springer, 457–468.

Knight VB., Serrano EE. (2017c). Post-translational Tubulin Modifications in Human Astrocyte Cultures. *Neurochemical Research*. DOI: 10.1007/s11064-017-2290-0.

Landis SC., Amara SG., Asadullah K., Austin CP., Blumenstein R., Bradley EW., Crystal RG., Darnell RB., Ferrante RJ., Fillit H., Finkelstein R., Fisher M., Gendelman HE., Golub RM., Goudreau JL., Gross RA., Gubitz AK., Hesterlee SE., Howells DW., Huguenard J., Kelner K., Koroshetz W., Krainc D., Lazic SE., Levine MS., Macleod MR., McCall JM., Moxley RT., Narasimhan K., Noble LJ., Perrin S., Porter JD., Steward O., Unger E., Utz U. & Silberberg SD. (2012). A call for transparent reporting to optimize the predictive value of preclinical research. *Nature* 490:187–191. DOI: 10.1038/nature11556.

Lee, M. K., Rebhun, L. I., & Frankfurter, A. (1990). Posttranslational modification of class III beta-tubulin. *Proceedings of the National Academy of Sciences of the United States of America*, *87*(18), 7195–7199. https://doi.org/10.1073/pnas.87.18.7195

Lessard, D. V., Zinder, O. J., Hotta, T., Verhey, K. J., Ohi, R., & Berger, C. L. (2019). Polyglutamylation of tubulin's C-terminal tail controls pausing and motility of kinesin-3 family member KIF1A. The Journal of biological chemistry, 294(16), 6353–6363. https://doi.org/10.1074/jbc.RA118.005765

Li L. & Yang XJ. (2015). Tubulin acetylation: Responsible enzymes, biological functions and human diseases. *Cellular and Molecular Life Sciences* 72:4237–4255. DOI: 10.1007/s00018-015-2000-5.

Matias, I., Morgado, J., & Gomes, F. (2019). Astrocyte Heterogeneity: Impact to Brain Aging and Disease. Frontiers in aging neuroscience, 11, 59. https://doi.org/10.3389/fnagi.2019.00059

Matyash V. & Kettenmann H. (2010). Heterogeneity in astrocyte morphology and physiology. *Brain Research Reviews* 63:2–10. DOI: 10.1016/j.brainresrev.2009.12.001.

Moody SA., Quigg MS. & Frankfurter A. (1989). Development of the peripheral trigeminal system in the chick revealed by an isotype-specific anti-beta-tubulin monoclonal antibody. *The Journal of Comparative Neurology* 279:567–580. DOI: 10.1002/cne.902790406.

Moutin, M. J., Bosc, C., Peris, L. & Andrieux, A. (2021). Tubulin post-translational modifications control neuronal development and functions. Developmental neurobiology, 81(3), 253–272. https://doi.org/10.1002/dneu.22774

Nedergaard M., Ransom B. & Goldman SA. (2003). New roles for astrocytes: Redefining the functional architecture of the brain. *Trends in Neurosciences* 26:523–530. DOI: 10.1016/j.tins.2003.08.008.

Oberheim NA., Takano T., Han X., He W., Lin JH., Wang F., Xu Q., Wyatt JD., Pilcher W., Ojemann JG., Ransom BR.,Goldman SA., & Nedergaard M. (2009). Uniquely hominid features of adult human astrocytes. *Journal of Neuroscience* 29:3276–3287. DOI: 10.1523/jneurosci.4707-08.2009.

Oikari LE., Okolicsanyi RK., Qin A., Yu C., Grif LR. & Haupt LM. (2016). Cell surface heparan sulfate proteoglycans as novel markers of human neural stem cell fate determination. 16:92–104. DOI: 10.1016/j.scr.2015.12.011.

Park, J. H., & Roll-Mecak, A. (2018). The tubulin code in neuronal polarity. *Current opinion in neurobiology*, *51*, 95–102. https://doi.org/10.1016/j.conb.2018.03.001

Pau G., Fuchs F., Sklyar O., Boutros M. & Huber W. (2010). EBImage-an R package for image processing with applications to cellular phenotypes. *Bioinformatics* 26:979–981. DOI: 10.1093/bioinformatics/btq046.

Pellegrini L., Wetzel A., Grannó S., Heaton G. & Harvey K. (2017). Back to the tubule: microtubule dynamics in Parkinson's disease. *Cellular and Molecular Life Sciences* 74:409–434. DOI: 10.1007/s00018-016-2351-6.

Przyborski, S. A., & Cambray-Deakin, M. A. (1997). Profile of glutamylated tubulin expression during cerebellar granule cell development in vitro. Brain research. Developmental brain research, 100(1), 133–138. https://doi.org/10.1016/s0165-3806(97)00031-x.

Roll-Mecak A. (2020). The Tubulin Code in Microtubule Dynamics and Information Encoding. *Developmental cell*, *54*(1), 7–20. https://doi.org/10.1016/j.devcel.2020.06.008

Romaniello, R., Arrigoni, F., Bassi, M. T., & Borgatti, R. (2015). Mutations in α- and β-tubulin encoding genes: implications in brain malformations. *Brain & development*, *37*(3), 273–280. https://doi.org/10.1016/j.braindev.2014.06.002.

Santiago-Mujika, E., Luthi-Carter, R., Giorgini, F., Kalaria, R. N., & Mukaetova-Ladinska, E. B. (2021). Tubulin and Tubulin Posttranslational Modifications in Alzheimer's Disease and Vascular Dementia. *Frontiers in aging neuroscience*, 13, 730107. https://doi.org/10.3389/fnagi.2021.730107.

Saragoni L., Hernández P. & Maccioni RB. (2000). Differential association of tau with subsets of microtubules containing posttranslationally-modified tubulin variants in neuroblastoma cells. *Neurochemical Research* 25:59–70. DOI: 10.1023/A:1007587315630.

Sheikh, A. M., Yano, S., Tabassum, S., Omura, K., Araki, A., Mitaki, S., Ito, Y., Huang, S., & Nagai, A. (2021). Alteration of Neural Stem Cell Functions in Ataxia and Male Sterility Mice: A Possible Role of β-Tubulin Glutamylation in Neurodegeneration. *Cells*, *10*(1), 155. https://doi.org/10.3390/cells10010155.

Schiweck, J., Eickholt, B. J., & Murk, K. (2018). Important Shapeshifter: Mechanisms Allowing Astrocytes to Respond to the Changing Nervous System During Development, Injury and Disease. *Frontiers in cellular neuroscienc*e, 12, 261. https://doi.org/10.3389/fncel.2018.00261.

Song Y. & Brady ST. (2015). Post-translational modifications of tubulin: Pathways to functional diversity of microtubules. *Trends in Cell Biology* 25:125–136. DOI: 10.1016/j.tcb.2014.10.004.

Stipursky J., De Sampaio e Spohr TCL., Sousa VO. & Gomes FCA. (2012). Neuron-astroglial interactions in cell-fate commitment and maturation in the central nervous system. *Neurochemical Research* 37:2402–2418. DOI: 10.1007/s11064-012-0798-x.

Tischfield MA., Cederquist GY., Gupta ML. & Engle EC. (2011). Phenotypic spectrum of the tubulin-related disorders and functional implications of disease-causing mutations. *Current Opinion in Genetics and Development* 21:286–294. DOI: 10.1016/j.gde.2011.01.003.

Vu HT., Akatsu H., Hashizume Y., Setou M. & Ikegami K. (2017). Increase in α -tubulin modifications in the neuronal processes of hippocampal neurons in both kainic acid-induced epileptic seizure and Alzheimer ' s disease. *Nature Publishing Group*:1–14. DOI: 10.1038/srep40205.

Wei D., Gao, N., Li, L., Zhu, J. X., Diao, L., Huang, J., Han, Q. J., Wang, S., Xue, H., Wang, Q., Wu, Q. F., Zhang, X., & Bao, L. (2018). α-Tubulin Acetylation Restricts Axon Overbranching by Dampening Microtubule Plus-End Dynamics in Neurons. Cerebral cortex (New York, N.Y. : 1991), 28(9), 3332–3346. https://doi.org/10.1093/cercor/bhx225.

Yoshiyama Y., Zhang B., Bruce J., Trojanowski JQ. & Lee VM-Y. (2003). Reduction of detyrosinated microtubules and Golgi fragmentation are linked to tau-induced degeneration in astrocytes. *The Journal of neuroscience : the official journal of the Society for Neuroscience* 23:10662–10671. DOI: 23/33/10662 [pii].

Youn GS., Ju SM., Choi SY. & Park J. (2015). HDAC6 mediates HIV-1 tat-induced proinflammatory responses by regulating MAPK-NF-kappaB/AP-1 pathways in astrocytes. *Glia* 63:1953–1965. DOI: 10.1002/glia.22865.

Zempel H., Luedtke J., Kumar Y., Biernat J., Dawson H., Mandelkow E. & Mandelkow E-M. (2013). Amyloid-β oligomers induce synaptic damage via Tau-dependent microtubule severing by TTLL6 and spastin. *The EMBO Journal* 32:2920–2937. DOI: 10.1038/emboj.2013.207.

Zhang Y., Kwon S., Yamaguchi T., Cubizolles F., Rousseaux S., Kneissel M., Cao C., Li N., Cheng H-L., Chua K., Lombard D., Mizeracki A., Matthias G., Alt FW., Khochbin S., & Matthias P. (2008). Mice Lacking Histone Deacetylase 6 Have Hyperacetylated Tubulin but Are Viable and Develop Normally. *Molecular and Cellular Biology* 28:1688–1701. DOI: 10.1128/MCB.01154-06.

Zhang F., Su B., Wang C., Siedlak SL., Mondragon-Rodriguez S., Lee H-G., Wang X., Perry G. & Zhu X. (2015). Posttranslational modifications of α-tubulin in alzheimer disease. *Translational neurodegeneration* 4:9. DOI: 10.1186/s40035-015-0030-4.

Zheng, P., Obara, C. J., Szczesna, E., Nixon-Abell, J., Mahalingan, K. K., Roll-Mecak, A., Lippincott-Schwartz, J., & Blackstone, C. (2021). ER proteins decipher the tubulin code to regulate organelle distribution. *Nature*, 10.1038/s41586-021-04204-9.